Structural Models for the Substrate−Catalyst Adduct in Hydrodenitrogenation Catalysis: Oxygen vs Sulfur Ligation

Peter A. Fox,† Michael A. Bruck, Steven D. Gray,‡ Nadine E. Gruhn, Carina Grittini, and David E. Wigley*

Carl S. Marvel Laboratories of Chemistry, Department of Chemistry, University of Arizona, Tucson, Arizona 85721-0041

Received July 2, 1997

A comparison between models for the substrate−catalyst adduct in hydrodenitrogenation (HDN) catalysis is made with respect to oxygen vs sulfur ancillary ligands. Reacting [η^2(*N*,*C*)-$NC_5{}^tBu_3H_2$]Ta(OAr)$_2$Cl (**1**, Ar = 2,6-$C_6H_3{}^iPr_2$) with KO^{t}Bu affords orange crystals of the alkoxide [η^2(*N*,*C*)-$NC_5{}^tBu_3H_2$]Ta(OAr)$_2$(O^{t}Bu) (**2**), while **1** and LiS^{t}Bu react to form the red thiolate analogue [η^2(*N*,*C*)-$NC_5{}^tBu_3H_2$]Ta(OAr)$_2$(S^{t}Bu) (**3**). Structural studies of both complexes **2** and **3** are reported and compared with other η^2(*N*,*C*)-$NC_5{}^tBu_3H_2$ derivatives. A trace of the bromide complex [η^2(*N*,*C*)-$NC_5{}^tBu_3H_2$]Ta(OAr)$_2$Br (**4**) is isolated from reacting [η^2(*N*,*C*)-$NC_5{}^tBu_3H_2$]Ta(OAr)$_2$Cl (**1**) with EtMgBr in THF/Et$_2$O solution and is also structurally characterized for comparison. Complexes **2**−**4** reveal a severe interruption of aromaticity within the heterocycle, different rotational preferences of the pyridine NC_5 plane with respect to the Ta(OAr)$_2$X moiety, and various aryloxide ligand structural differences. From this comparison, arguments will be presented that support the ancillary ligand π-donor ability decreasing as O^{t}Bu > OAr > S^{t}Bu > Cl ≈ Br > Et, although evidence suggests that the S^{t}Bu ligand is a better $\sigma + \pi$ donor overall than OAr or O^{t}Bu.

Introduction

One major goal of hydrotreating petroleum and coal-derived liquids is the catalytic removal of nitrogen-containing impurities from these feedstocks.[1,2] Hydrodenitrogenation (HDN) is generally effected over sulfided CoMo/γ-Al_2O_3 or NiMo/γ-Al_2O_3 under rather severe hydrogenation conditions (350−500 °C and up to 200 atm of H_2) that ultimately remove the nitrogen as NH_3.[3,4] These catalysts are typically prepared by impregnating γ-Al_2O_3 with aqueous solutions of [NH_4]$_6$[Mo_7O_{24}], along with a nickel or cobalt promotor such as Co(NO_3)$_3$.[4] The impregnating alumina is first calcined to afford oxide phases and then sulfided (with H_2S, thiophene, or simply a sulfur-rich feed) to generate the active hydrotreating catalyst. The most active catalytic site appears to be crystallites of MoS_2 supported on γ-alumina, with Co atoms adsorbed along the edges of the layered MoS_2 structure.[4] A Mo−S site of this "CoMoS" phase is usually associated with nitrogen substrate activation, and hydrogen is often described as dissociatively bound to sulfur in the form of sulfhydryl groups,[3−5] while the role of the cocatalyst remains debatable.[5,6]

Of all the nitrogen compounds subject to hydrodenitrogenation catalysis[5,7,8] during petroleum refining, the basic heterocyclic compounds that contain pyridine rings are among the most difficult to convert.[3,9−11] We recently described HDN model studies in which C−N bond cleavage was achieved in a coordinated pyridine ligand and led to a cascade of subsequent heterocycle rearrangement and degradation reactions.[12−16] In all cases reported thus far, heterocycle bond scission has been observed only in η^2(*N*,*C*)-bound pyridine ligands, and η^2(*N*,*C*)-heterocycles are observed only in the d^2 oxidation state.[12−17] This remarkable heterocycle activation constitutes a valuable reactivity model for fun-

† Present Address: Department of Chemistry, Stanford University, Stanford, CA 94305.

‡ Present Address: Fina Oil and Chemical Company, P.O. Box 1200, Hiway 134 at Miller Cutoff, Deer Park, TX 77536.

(1) Satterfield, C. N. *Heterogeneous Catalysis in Industrial Practice,* 2nd ed.; McGraw-Hill: New York, 1991.
(2) Gary, J. H.; Handwerk, G. E. *Petroleum Refining: Technology and Economics* 3rd ed.; Marcel Dekker: New York, 1993.
(3) Katzer, J. R.; Sivasubramanian, R. *Catal. Rev.-Sci. Eng.* **1979**, *20*, 155.
(4) Prins, R.; de Beer, V. H. J.; Somorjai, G. A. *Catal. Rev.-Sci. Eng.* **1989**, *31*, 1.
(5) Ho, T. C. *Catal. Rev.-Sci. Eng.* **1988**, *30*, 117.
(6) Harris, S.; Chianelli, R. R. *J. Catal.* **1986**, *98*, 17.
(7) Angelici, R. J. In *Encyclopedia of Inorganic Chemistry*; King, R. B., Ed.; John Wiley and Sons: New York, 1994; Vol. 3, pp 1433−1443.
(8) Ledoux, M. J. In *Catalysis*; The Chemical Society, London, 1988; Vol. 7, pp 125−148.
(9) Laine, R. M. *Catal. Rev.-Sci. Eng.* **1983**, *25*, 459.
(10) Laine, R. M. *Ann. NY Acad. Sci.* **1983**, *415*, 271.
(11) Fish, R. H. *Ann. NY Acad. Sci.* **1983**, *415*, 292.
(12) Gray, S. D.; Smith, D. P.; Bruck, M. A.; Wigley, D. E. *J. Am. Chem. Soc.* **1992**, *114*, 5462.
(13) Gray, S. D.; Weller, K. J.; Bruck, M. A.; Briggs, P. M.; Wigley, D. E. *J. Am. Chem. Soc.* **1995**, *117*, 10678.
(14) Weller, K. J.; Gray, S. D.; Briggs, P. M.; Wigley, D. E. *Organometallics* **1995**, *14*, 5588.
(15) Weller, K. J.; Fox, P. A.; Gray, S. D.; Wigley, D. E. *Polyhedron* **1997**, *16*, 3139.
(16) Weller, K. J.; Filippov, I.; Briggs, P. M.; Wigley, D. E. *J. Organomet. Chem.* **1997**, *528*, 225.
(17) Kleckley, T. S.; Bennett, J. L.; Wolczanski, P. T.; Lobkovsky, E. B. *J. Am. Chem. Soc.* **1997**, *119*, 247.

S0276-7333(97)00559-1 CCC: $15.00
Publication on Web 06/05/1998

Scheme 1

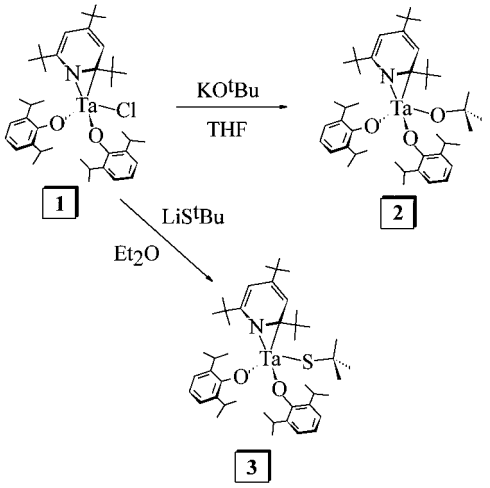

damental HDN chemistry and mandates a further examination of the substituent effects on $\eta^2(N,C)$ bonding.

In this report, we prepare and characterize structural models for the substrate−catalyst adduct in hydrodenitrogenation catalysis, viz. $[\eta^2(N,C)\text{-}NC_5{}^tBu_3H_2]Ta(OAr)_2X$, where X = O^{t}Bu and S^{t}Bu. We also include the bromide complex $[\eta^2(N,C)\text{-}NC_5{}^tBu_3H_2]Ta(OAr)_2Br$ in this structural analysis. Along with previously reported $\eta^2(N,C)$-pyridine species, these complexes allow a direct comparison of the influence of oxygen vs sulfur ligation in effecting pyridine ligand activation.

Results

Preparation and Properties of Model Substrate−Catalyst Complexes. The $\eta^2(N,C)$-pyridine complex $[\eta^2(N,C)\text{-}NC_5{}^tBu_3H_2]Ta(OAr)_2Cl$ (**1**, Ar = 2,6-$C_6H_3{}^iPr_2$) is prepared by the cycloaddition methodology previously described.[18] Reacting $[\eta^2(N,C)\text{-}NC_5{}^tBu_3H_2]Ta(OAr)_2Cl$ (**1**) with 1 equiv of KO^{t}Bu (in THF) affords orange crystals of the *tert*-butoxide complex $[\eta^2(N,C)\text{-}NC_5{}^tBu_3H_2]Ta(OAr)_2(O^tBu)$ (**2**) in good yield, after appropriate workup, Scheme 1. Likewise, the reaction of **1** with 1 equiv of LiS^{t}Bu (in Et_2O) provides a moderate to good yield of $[\eta^2(N,C)\text{-}NC_5{}^tBu_3H_2]Ta(OAr)_2(S^tBu)$ (**3**), isolated as red crystals after workup, Scheme 1. Both complexes are extremely ether soluble, therefore analytically pure, high-quality crystals were obtained by layering acetonitrile on solutions of **1** and **2** dissolved in a minimal volume of Et_2O.

In contrast to their chloride precursor **1**[18] and the alkyl derivatives $[\eta^2(N,C)\text{-}NC_5{}^tBu_3H_2]Ta(OAr)_2R$,[13] both **2** and **3** exhibit *static* $\eta^2(N,C)$-pyridine ligands at room temperature according to their ^{1}H NMR spectra. As suggested by the structures in Scheme 1, the absence of a molecular symmetry plane renders the pyridine ring protons, the pyridine ring carbons, and the aryloxide ligands inequivalent in a rigid structure. In $[\eta^2(N,C)\text{-}NC_5{}^tBu_3H_2]Ta(OAr)_2(O^tBu)$ (**2**), the pyridine ring protons resonate at δ 6.05 and 5.46 (in C_6D_6) and at δ 6.36 and 5.52 in $[\eta^2(N,C)\text{-}NC_5{}^tBu_3H_2]Ta(OAr)_2(S^tBu)$ (**3**). At 60 °C, the ring protons of **3** have not detectably broadened (toluene-d_8), indicating an intact static structure. These data can be compared to the broad singlet at δ 5.63 for the pyridine protons of $[\eta^2(N,C)\text{-}C_5{}^tBu_3H_2]Ta(OAr)_2Me$ that are equilibrating at room temperature by an intramolecular exchange process. This equilibration is proposed to occur by "ring rocking" in which the pyridine ortho carbons alternately dissociate from, and then recoordinate, the metal center, eq 1.[13] At −90 °C in toluene-d_8, the ring-rocking process

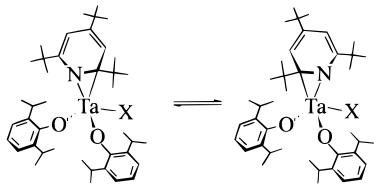

(1)

in $[\eta^2(N,C)\text{-}NC_5{}^tBu_3H_2]Ta(OAr)_2Me$ is slowed and their resonances in a static pyridine ligand appear at δ 5.73 and 5.50.[13]

Crystals of the bromide complex $[\eta^2(N,C)\text{-}NC_5{}^tBu_3H_2]Ta(OAr)_2Br$ (**4**) can be isolated in very low yield from the reaction of $[\eta^2(N,C)\text{-}NC_5{}^tBu_3H_2]Ta(OAr)_2Cl$ (**1**) with EtMgBr in THF/Et_2O solution. The major product of this reaction, $[\eta^2(N,C)\text{-}NC_5{}^tBu_3H_2]Ta(OAr)_2Et$ (**5**), has been described in detail.[13] Thus, the oil obtained from the **1** + EtMgBr reaction is shown to consist almost entirely of the ethyl derivative **4**, which must be crystallized from concentrated Et_2O/MeCN solutions. However, a few crystals of $[\eta^2(N,C)\text{-}NC_5{}^tBu_3H_2]Ta(OAr)_2Br$ (**4**) are isolated by dissolving this oil in pentane and cooling the sample to −35 °C for 3 days. We took this opportunity to include the structural determination of **4** in this comparison study.

Structural Studies of Model Substrate−Catalyst Complexes. Orange, block-shaped crystals of $[\eta^2(N,C)\text{-}NC_5{}^tBu_3H_2]Ta(OAr)_2(O^tBu)$ (**2**) and red, block-shaped crystals of $[\eta^2(N,C)\text{-}NC_5{}^tBu_3H_2]Ta(OAr)_2(S^tBu)$ (**3**) suitable for an X-ray structural study were grown from Et_2O/MeCN solutions at −35 °C. Crystals of the bromide complex $[\eta^2(N,C)\text{-}NC_5{}^tBu_3H_2]Ta(OAr)_2Br$ (**4**) were obtained from pentane solutions at −35 °C. A summary of the crystal data and structural analysis of these compounds are given in Table 1, and relevant bond distances, bond angles, and torsion angles are provided in Table 2. Figures 1, 2, and 3 present drawings of $[\eta^2(N,C)\text{-}NC_5{}^tBu_3H_2]Ta(OAr)_2(O^tBu)$ (**2**), $[\eta^2(N,C)\text{-}NC_5{}^tBu_3H_2]Ta(OAr)_2(S^tBu)$ (**3**), and $[\eta^2(N,C)\text{-}NC_5{}^tBu_3H_2]Ta(OAr)_2Br$ (**4**), respectively, while the core structures of all three molecules are shown in Figure 4. The structural determination of $[\eta^2(N,C)\text{-}NC_5{}^tBu_3H_2]Ta(OAr)_2(O^tBu)$ (**2**) was the most precise of the three structures examined and, therefore, will be discussed in some detail.

$[\eta^2(N,C)\text{-}NC_5{}^tBu_3H_2]Ta(OAr)_2(O^tBu)$ (2). The molecular structure of compound **2** unambiguously establishes the $\eta^2(N,C)$ binding mode of the pyridine ligand. The overall complex can be described as a distorted tetrahedron if the N−C(1) bond is considered as occupying a single coordination site. The tantalum−pyridine interaction in **2** features a Ta−N bond of 1.958(3) Å and Ta−C(1) distance of 2.163(3) Å, similar to the structures of $[\eta^2(N,C)\text{-}NC_5{}^tBu_3H_2]Ta(OAr)_2X$ for X = Cl[18] and X = Et.[13] The N−C(1) distance of 1.471(4) Å supports the

(18) Smith, D. P.; Strickler, J. R.; Gray, S. D.; Bruck, M. A.; Holmes, R. S.; Wigley, D. E. *Organometallics* **1992**, *11*, 1275.

Table 1. Details of the X-ray Diffraction Studies for [η^2(*N*,*C*)-$NC_5{}^tBu_3H_2$]Ta(OAr)$_2$X (2, X = O^{t}Bu; 3, X = S^{t}Bu; 4, X = Br)

	[η^2(*N*,*C*)$NC_5{}^tBu_3H_2$]Ta(OAr)$_2$(O^{t}Bu) (**2**)	[η^2(*N*,*C*)$NC_5{}^tBu_3H_2$]Ta(OAr)$_2$(S^{t}Bu) (**3**)	[η^2(*N*,*C*)-$NC_5{}^tBu_3H_2$]Ta(OAr)$_2$Br (**4**)
		Crystal Parameters	
mol formula	$C_{45}H_{72}NO_3Ta$	$C_{45}H_{72}NO_2STa$	$C_{41}H_{63}BrNO_2Ta$
mol wt	856.03	872.09	862.82
F(000)	1784	1816	1760
cryst color	orange	red	dark red
space group	monoclinic $P2_1/n$ (No. 14)	orthorhombic $P2_12_12_1$ (No. 19)	orthorhombic $Pca2_1$ (No. 29)
unit cell volume, Å^3	4400(1)	4571.1(6)	4152.0
a, Å	11.945(2)	11.893(1)	20.691(1)
b, Å	21.216(4)	19.061(1)	10.109(1)
c, Å	17.434(2)	20.165(1)	19.851(1)
β, deg	95.27(1)°		
Z	4	4	4
D(calc), g cm^{-3}	1.29	1.26	1.38
cryst dimens, mm	0.33 × 0.33 × 0.50	0.17 × 0.27 × 0.28	0.20 × 0.20 × 0.30
ω width, deg	0.37	0.25	0.25
abs coeff, cm^{-1}	25.0	24.5	36.0
data collection temp, °C	−70 ± 1	20 ± 1	23 ± 1
		Data Collection	
diffractometer	Enraf-Nonius CAD4	Enraf-Nonius CAD4	Enraf-Nonius CAD4
monochromator	graphite crystal, incident beam	graphite crystal, incident beam	graphite crystal, incident beam
Mo Kα radiation, λ, Å	0.710 73	0.710 73	0.710 73
2θ range, deg	2−50	2−50	2−50
octants collected	$+h, +k, \pm l$	$+h, +k, +l$	$+h, +k, +l$
scan type	ω−2θ	ω−2θ	ω−2θ
scan speed, deg min^{-1}	4−7	1−7	1−7
scan width, deg	0.8 + 0.340 tan θ	0.8 + 0.340 tan θ	0.6 + 0.340 tan θ
total no. of reflns measd	8363 (7711 unique)	4492 (4462 unique)	4111 (3759 unique)
corrections	Lorentz−polarization ψ-scan absorption (min 0.957, max 0.999, avg 0.981) reflection averaging (agreement on I = 2.7%)	Lorentz−polarization ψ-scan absorption (min 0.812, max 1.000, avg 0.952)	Lorentz−polarization
		Solution and Refinement	
solution	Patterson method	Patterson method	Patterson method
refinement	full-matrix least-squares	full-matrix least-squares	full-matrix least-squares
minimization function	$\sum w(\|F_o\| - \|F_c\|)^2$	$\sum w(\|F_o\| - \|F_c\|)^2$	$\sum w(\|F_o\| - \|F_c\|)^2$
no. of reflns used in refinement; $I > 3\sigma(I)$	6333	3757	3099
no. of param refined	451	451	414
R ($\sum\|\|F_o\| - \|F_c\|\|/\sum\|F_o\|$)	0.025	0.036	0.039
R_w ($[\sum w(\|F_o\| - \|F_c\|)^2/\sum w(F_o)^2]^{1/2}$)	0.033	0.046	0.055
esd of obs of unit weight	1.25	1.69	2.16
convergence, largest shift	0.00σ	0.08σ	0.12σ
Δ/σ(max), e^{-1}/Å^3	1.38(8)	1.53(9)	2.08(12)
Δ/σ(min), e^{-1}/Å^3	0.15(8)	−0.15(9)	−0.21(12)
computer hardware	VAX	VAX	VAX
computer software	MolEN (Enraf-Nonius)	MolEN (Enraf-Nonius)	MolEN (Enraf-Nonius)

Table 2. Selected Bond Distances (Å), Bond Angles (deg), and Torsion Angles (deg) in [η^2(*N,C*)-$NC_5{}^tBu_3H_2$]Ta(OAr)$_2$X (2, X = O^{t}Bu; 3, X = S^{t}Bu; 4, X = Br)[a]

	X = O^{t}Bu (2)	X = S^{t}Bu (3)	X = Br (4)
	Bond Distances		
N−C(1)	1.471(4)	1.46(1)	1.42(2)
C(1)−C(2)	1.476(5)	1.44(1)	1.49(2)
C(2)−C(3)	1.350(6)	1.31(1)	1.33(2)
C(3)−C(4)	1.451(5)	1.45(2)	1.43(2)
C(4)−C(5)	1.344(5)	1.32(1)	1.36(2)
C(5)−N	1.408(5)	1.43(1)	1.39(1)
Ta−N	1.958(3)	1.969(8)	1.95(1)
Ta−C(1)	2.163(3)	2.24(1)	2.16(1)
Ta−X	1.844(3)	2.356(3)	2.496(2)
Ta−O(10)	1.905(2)	1.871(6)	1.80(1)
Ta−O(20)	1.918(2)	1.873(6)	1.893(9)
X−C(6A)	1.445(4)	1.85(1)	
	Bond Angles		
X−Ta−O(10)	113.5(1)	102.8(2)	94.3(3)
X−Ta−O(20)	103.1(1)	109.3(2)	101.4(3)
O(10)−Ta−O(20)	98.4(1)	110.2(3)	119.8(4)
C,N[b]−Ta−O(10)	114	120	119
C,N[b]−Ta−O(20)	115	112	109
C,N[b]−Ta−X	110	100	109
Ta−C(1)−C(2)	114.1(2)	109.9(7)	114.0(9)
Ta−N−C(5)	140.9(2)	132.3(6)	122.(1)
Ta−C(1)−N	61.8(2)	60.1(5)	62.4(7)
Ta−N−C(1)	76.8(2)	79.8(6)	77.7(8)
C(1)−Ta−N	41.4(1)	40.1(3)	39.9(6)
Ta−E(O or S)−C(6)	169.1(2)	112.8(4)	
Ta−O(10)−C(11)	147.1(2)	164.6(6)	163.6(9)
Ta−O(20)−C(21)	153.1(2)	162.0(7)	167.6(9)
	Torsion Angles		
C(1)−C(2)−C(3)−C(4)	1.25(53)	0.12(149)	−3.43(211)
C(2)−C(3)−C(4)−C(5)	14.12(55)	12.42(147)	12.85(208)
C(3)−C(4)−C(5)−N	−3.38(53)	−1.19(139)	1.95(184)
C(4)−C(5)−N−C(1)	−22.50(46)	−21.83(120)	−27.70(149)
C(5)−N−C(1)−C(2)	34.84(40)	31.71(104)	34.59(142)
N−C(1)−C(2)−C(3)	−23.81(46)	−20.87(128)	−18.40(182)

[a] Numbers in parentheses are estimated standard deviations in the least significant digits. [b] C,N represents the midpoint of the C(2)−N bond; uncertainties are not calculated for these values.

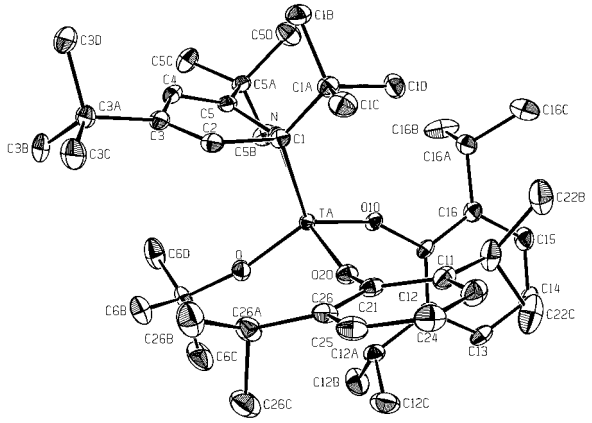

Figure 1. ORTEP drawing of [η^2(*N,C*)-$NC_5{}^tBu_3H_2$]-Ta(OAr)$_2$(O^{t}Bu) (**2**) with atoms shown as 30% probability ellipsoids.

Ta(V) metallaaziridine[19,20] description of **2**, reflecting a driving force for tantalum to attain its highest oxidation state. No other close approaches of the remaining atoms of the pyridine ligand to the metal were observed. The

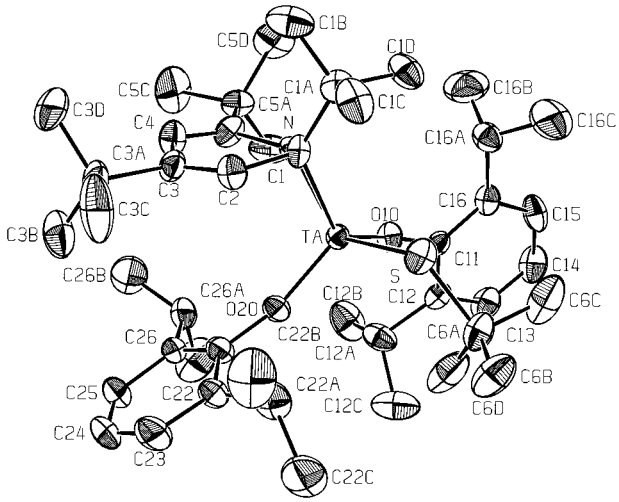

Figure 2. ORTEP drawing of [η^2(*N,C*)-$NC_5{}^tBu_3H_2$]-Ta(OAr)$_2$(S^{t}Bu) (**3**) with atoms shown as 30% probability ellipsoids.

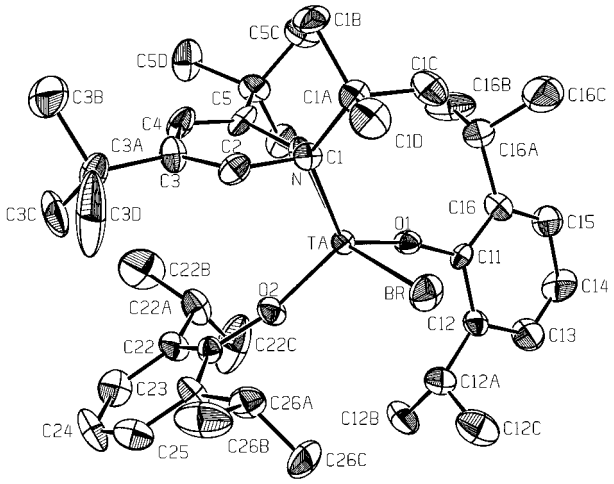

Figure 3. ORTEP drawing of [η^2(*N,C*)-$NC_5{}^tBu_3H_2$]Ta(OAr)$_2$-Br (**4**) with atoms shown as 30% probability ellipsoids.

pyridine ligand is somewhat distorted toward a twist-boat conformation (in contrast to the planar pyridine in [η^2(*N,C*)-NC_5H_5]Ta(OSi^{t}Bu$_3$)$_3$[21,22]), however, the angle between the *best* pyridine plane and the Ta−N−C(1) plane is 121.94 ± 0.14°. Additionally, a 1,3-diene-type π-electron localization is readily apparent in the η^2-pyridine of **2** as the C(2)−C(3) and C(4)−C(5) bonds (average 1.35 Å) are much shorter than the C(1)−C(2) and C(3)−C(4) bonds (average 1.46 Å). The torsion angles around the pyridine ring are consistent with this picture: the C(1)−C(2)−C(3)−C(4) and C(3)−C(4)−C(5)−N torsion angles are near 0°, as expected for C(2)−C(3) and C(4)−C(5) double bonds, respectively, Table 2. The other pyridine torsion angles are much larger, indicating a significant deviation from planarity, which further substantiates π localization of the heterocycle. An interruption of aromaticity of this type has been noted in all of the coordinated η^2(*N,C*)-pyridine rings structurally characterized to date: [η^2(*N,C*)-NC_5H_5]-Ta(OSi^{t}Bu$_3$)$_3$;[21,22] the 6-methylquinoline derivatives [η^2-

(19) Durfee, L. D.; Fanwick, P. E.; Rothwell, I. P.; Folting, K.; Huffman, J. C. *J. Am. Chem. Soc.* **1987**, *109*, 4720.
(20) Durfee, L. D.; Hill, J. E.; Kerschner, J. L.; Fanwick, P. E.; Rothwell, I. P. *Inorg. Chem.* **1989**, *28*, 3095.
(21) Neithamer, D. R.; Párkányi, L.; Mitchell, J. F.; Wolczanski, P. T. *J. Am. Chem. Soc.* **1988**, *110*, 4421.
(22) Covert, K. J.; Neithamer, D. R.; Zonnevylle, M. C.; LaPointe, R. E.; Schaller, C. P.; Wolczanski, P. T. *Inorg. Chem.* **1991**, *30*, 2494.

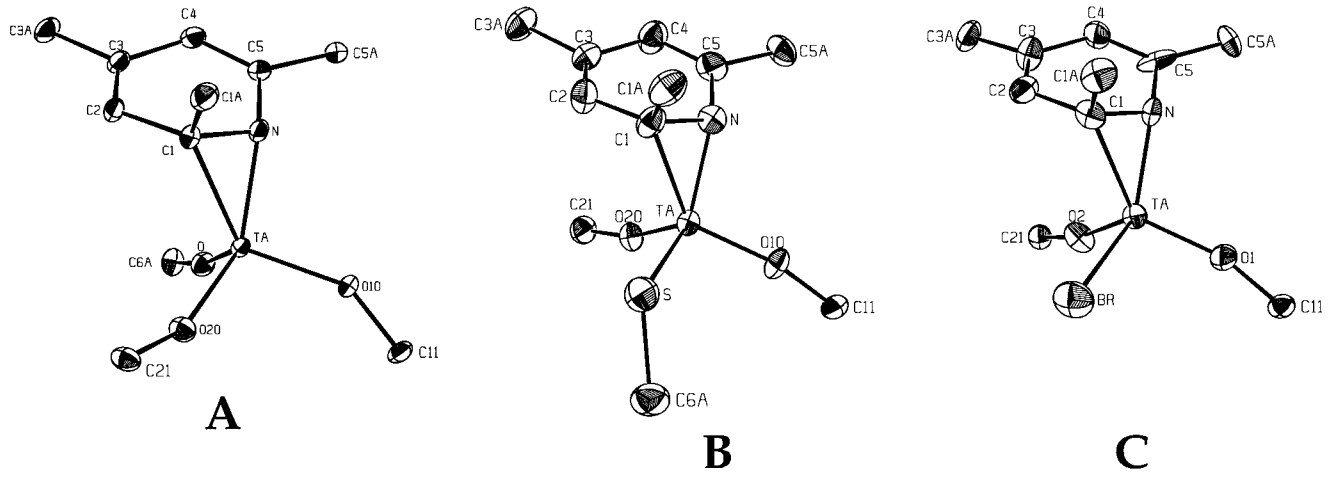

Figure 4. Core structures of (A) $[\eta^2(N,C)\text{-}NC_5{}^tBu_3H_2]Ta(OAr)_2(O^tBu)$ (**2**), (B) $[\eta^2(N,C)\text{-}NC_5{}^tBu_3H_2]Ta(OAr)_2(S^tBu)$ (**3**), and (C) $[\eta^2(N,C)\text{-}NC_5{}^tBu_3H_2]Ta(OAr)_2Br$ (**4**) with atoms shown as 30% probability ellipsoids.

(N,C)-$NC_{10}H_9]Ta(OAr)_3(PMe_3)$ and $[\eta^2(N,C)$-$NC_{10}H_9]Ta(OAr)_2Cl(OEt_2)$;[23] and in $[\eta^2(N,C)$-$NC_5{}^tBu_3H_2]Ta(OAr)_2X$ (X = Cl[18] and Et[13]).

The planes of the aryloxide ligands are situated roughly perpendicular to each other (dihedral angle 96.74(13)°) in an orientation that places the isopropyl groups in an efficient packing arrangement about the molecule. The O^{t}Bu ligand is characterized by a Ta−O−C(6a) angle of 169.1(2)°, which is significantly larger than the Ta−O−C angles of the aryloxide ligands (average 150°), Table 2. While there is considerable steric flexibility in the alkoxide ligand M−O−C angles, this difference between the aryloxide vs alkoxide ligands has been attributed to the less efficient π donation of the aryloxide ligands, a difference that may arise from interaction of one of the orthogonal O(2p) orbitals with the arene π system.[24] Finally, we note that the C(1)−N bond of the η^2-pyridine lies nearly parallel to one of the tantalum−aryloxide bonds (Ta−O(20)). This orientation places the *tert*-butoxide group beneath the η^2-pyridine ligand, roughly eclipsing the C(3)−C(4) bond when viewed perpendicular to the best pyridine plane.

$[\eta^2(N,C)$-$NC_5{}^tBu_3H_2]Ta(OAr)_2(S^tBu)$ (3). As shown in Figures 2 and 4 and in Table 2, the structural distortions of the $\eta^2(N,C)$-pyridine ligand in compound **3** are very similar to those described above for **2**. The short Ta−N (1.969(8) Å) and Ta−C(1) (2.24(1) Å) bonds, the long N−C(1) distance (1.46(1) Å), the 1,3-diene-like π localization within the twisted pyridine ring, and the 115.16 ± 0.26° angle between the best pyridine plane and the Ta−N−C(1) plane in $[\eta^2(N,C)$-$NC_5{}^tBu_3H_2]$-$Ta(OAr)_2(S^tBu)$ (**3**) are all similar to the structural distortions found in the pyridine ligands of **1**, **2**, and **4**. The torsion angles about the pyridine ring also indicate π localization and a disruption of aromaticity, Table 2. The S^{t}Bu ligand is characterized by a Ta−S−C(6a) angle of 112.8(4)°, which is much smaller than the Ta−O−C angles of the aryloxide ligands (average 163°) and significantly more acute than the Ta−O−C(6a) angle (169.1(2)°) of the *tert*-butoxide ligand in compound **2**, Table 2. Note that the 163° average aryloxide Ta−O−C_{ipso} bond angle in $[\eta^2(N,C)$-$NC_5{}^tBu_3H_2]Ta(OAr)_2(S^tBu)$ (**3**) is much greater than the 150° average aryloxide Ta−O−C_{ipso} angle in the *tert*-butoxide derivative **2**. As in complex **2**, the planes of the aryloxide ligands in **3** are oriented roughly perpendicular to each other, which constitutes an efficient packing arrangement of the isopropyl groups of these ligands. The pyridine ligand orientation with respect to the TaO_2X tripod in complex **3** (X = S) differs from that in the *tert*-butoxide complex **2**. The C(1)−N bond of the η^2-pyridine in the S^{t}Bu complex **3** lies roughly parallel to the Ta−S bond, which places an aryloxide ligand under the pyridine ring, when viewed normal to the best pyridine plane.

$[\eta^2(N,C)$-$NC_5{}^tBu_3H_2]Ta(OAr)_2Br$ (4). Although the structural determination of **4** is not as precise as those of **2** or **3**, it is clear that the perturbations of the pyridine ligand in this bromide derivative mirror those of compounds **2** and **3**: Ta−N = 1.95(1) Å and Ta−C(1) = 2.16(1) Å; the N−C(1) distance is quite long (1.42(2) Å); a distinct diene-like π localization exists within a twisted pyridine ring; and there is a 119.18 ± 0.43° angle between the best pyridine plane and the Ta−N−C(1) plane in compound **4**. The pyridine ligand orientation with respect to the TaO_2Br tripod is almost identical to the chloride analogue **1**,[18] i.e., the C(1)−N bond of the η^2-pyridine lies roughly parallel to the Ta−Br bond.

Bond Length/Bond Angle Comparisons Among $\eta^2(N,C)$-Pyridine Complexes. Table 2 allows a ready comparison of the bond angles and distances among these three complexes. We will focus mainly on comparing the O^{t}Bu complex (**2**) and the S^{t}Bu complex (**3**) since their structural data are the more precise. Although the structures of **2** and **3** share many similar features, when compared directly, some striking differences emerge. The Ta−C(1) bond length is significantly longer in the S^{t}Bu complex (2.24(1) Å) vs the O^{t}Bu derivative (2.163(3) Å), although their Ta−N bond lengths are essentially the same. This fact may be related to the observation that donor ligands (including π-bonded ligands) are typically more loosely bound in high-oxidation-state thiolate complexes as compared to their alkoxide homologues.[25−27] This observation has been explained on the basis of a greater donor ability

(23) Allen, K. D.; Bruck, M. A.; Gray, S. D.; Kingsborough, R. P.; Smith, D. P.; Weller, K. J.; Wigley, D. E. *Polyhedron* **1995**, *14*, 3315.
(24) Coffindaffer, T. W.; Rothwell, I. P.; Huffman, J. C. *Inorg. Chem.* **1983**, *22*, 2906.

Table 3. Key Structural Data for the Compounds [η^2(*N,C*)-$NC_5{}^tBu_3H_2$]Ta$(OAr)_2X$ (1, X = Cl; 2, X = O^{t}Bu; 3, X = S^{t}Bu; 4, X = Br; 5, X = Et)

compound	r_X (Å)[a]	$r_{Ta} = d_{Ta-X} - r_X$ (Å)[a]	torsion ligand L	C(1)−N-Ta-L torsion angle (deg)	C(5)−N-C(1)−C(2) torsion angle (deg)	Ta−C(1) (Å)
1, X = Cl	0.99[b]	1.35	Cl	27.5(9)	36.6(13)	2.133(3)
2, X = O^{t}Bu	0.68[c]	1.16	OAr[d]	15.5(2)	38.8(4)	2.163(3)
3, X = S^{t}Bu	1.08[c]	1.28	S^{t}Bu	31.8(4)	31.7(10)	2.24(1)
4, X = Br	1.14[b]	1.36	Br	26.3(7)	34.6(14)	2.16(1)
5, X = Et	0.77[c]	1.43	OAr[d]	−5.0(5)	37.0(8)	2.152(7)

[a] r_X = covalent radius of X; r_{Ta} = calculated covalent radius of Ta, assuming Ta−X single bond only; d_{Ta-X} from Table 2 and refs 13 and 18. [b] From ref 28. [c] See text. [d] OAr = O(20) for **2** and O(10) for **5**.

(σ and possibly π) of the thiolate vs the alkoxide ligand,[25−27] a possibility that will be discussed further below.

The large Ta−O−C(6a) angle (169.1(2)°) of the O^{t}Bu ligand in **2** as compared to the small Ta−S−C(6a) angle (112.8(4)°) of the S^{t}Bu ligand in **3** mirrors the trend observed in the bond angles of H_2O (104.5°) and H_2S (92.1°) and is usually interpreted as the diminished use of hybrid orbitals (therefore p orbital bonding only) in elements below period 2.[28] The Ta−O−C_{ipso} bond angles in the aryloxide ligands are very similar in the S^{t}Bu (**3**) and Br (**4**) complexes (roughly 164°) but considerably smaller in the O^{t}Bu complex **2** (about 150°). Additionally, the aryloxide Ta−O bond lengths are quite similar in the S^{t}Bu (**3**) and Br (**4**) complexes (average 1.86 Å) but considerably longer in the O^{t}Bu complex **2** (average 1.91 Å). These data seem to suggest a greater π-donating ability of O^{t}Bu vs S^{t}Bu or Br ligands in these complexes. In complex **3** where S^{t}Bu presumably donates less π-electron density to the metal than O^{t}Bu does in **2**, the aryloxide ligands appear to compensate for this loss by increasing their π-electron donation, as evidenced by the shorter Ta−O(10) and Ta−O(20) bonds in complex **3** as compared to **2**.[29] Rothwell has used such structural data in niobium[30] and tungsten[31] aryloxide complexes to correlate M−O bond lengths to the valence-electron count at the metal center. While metal−alkoxide bond lengths may be used (with caution!) to measure combined $\sigma + \pi$ donation in these ligands,[29,32] Rothwell has suggested that M−O−C angles show no correlation to M−O bond distances in aryloxide complexes and, therefore, are presumed to be unreliable indicators of the π-donating ability of these ligands.[33]

We can obtain some measure of the π-donating abilities of the O^{t}Bu and S^{t}Bu ligands by comparing the observed Ta−O and Ta−S bond distances with calculated or predicted Ta−O and Ta−S *single*-bond lengths. The Ta−C(sp^3) distance in [η^2(*N,C*)-$NC_5{}^tBu_3H_2$]Ta$(OAr)_2$-Et (**5**) is observed to be 2.20(13) Å, therefore if we assume $r_{C(sp^3)} = 0.77$ Å, then we can calculate $r_{Ta} = 1.43$ Å and use this value as a standard in all of these complexes. Likewise, estimating r_S from $d_{S-C} = r_S + r_{C(sp^3)}$ in the S^{t}Bu ligand in **3**, we obtain $r_S = 1.08$. The Ta−S single bond d_{Ta-S} can, therefore, be calculated as $r_{Ta} + r_S = 2.51$ Å, as compared to the *observed* d_{Ta-S} of 2.356(3) Å. Similar considerations provide a *calculated* $d_{Ta-O} = 2.11$ Å (based upon an estimated $r_O = 0.68$ Å) as compared to the *observed* $d_{Ta-O} = 1.844(3)$ Å. Thus, the *tert*-butoxide Ta−O bond is ca. 13% shorter than predicted on the basis of single bonding only, while the *tert*-butyl thiolate Ta−S bond is ca. 6% shorter than expected.[34] However, as Chisholm has pointed out, the difference in orbital energies between an electropositive metal center and oxygen will result in a small π bond order and relatively little π-electron density actually shifted to the metal from the oxygen.[29,32] A similar structural method that compares M−O vs M−C distances has been used to examine π-donor abilities in groups 4,[35] 13,[36] and 14[35] aryloxide complexes.

If one applies these simple bond length considerations to all compounds **1**−**5**, then *on the basis of single bonding only*, the values of r_{Ta} calculated from $r_{Ta} = d_{Ta-X} - r_X$ should be nearly identical. These r_{Ta} values are reported in Table 3, along with a value of r_X used in each calculation. If one assumes that this trend in "apparent" r_{Ta} values is related to the extent of π donation of each of the ancillary ligands X in compounds **1**−**5**, then the π-donor ability is observed to decrease as O^{t}Bu > OAr > S^{t}Bu > Cl ≈ Br > Et.

Pyridine Ligand Orientation Comparisons Among η^2(*N,C*)-Pyridine Complexes. We previously reported[13,18] the structures of [η^2(*N,C*)-$NC_5{}^tBu_3H_2$]-Ta$(OAr)_2$Et (**5**) and [η^2(*N,C*)-$NC_5{}^tBu_3H_2$]Ta$(OAr)_2$Cl (**1**), which indicated little overall change had occurred in the pyridine ligand upon alkylation of complex **1**, although the relative orientation of the pyridine ligand with respect to the Ta$(OAr)_2$X tripod (X = Cl or Et) differs. This rotational preference of the pyridine C−N bond is reflected in the chloride substituent in [η^2(*N,C*)-$NC_5{}^t$-Bu_3H_2]Ta$(OAr)_2$Cl (**1**) being situated proximate to C(1) while the ethyl substituent in [η^2(*N,C*)-$NC_5{}^tBu_3H_2$]-

(25) Walborsky, E. C.; Wigley, D. E.; Roland, E.; Dewan, J. C.; Schrock, R. R. *Inorg. Chem.* **1987**, *26*, 1615.
(26) Wallace, K. C.; Liu, A. H.; Dewan, J. C.; Schrock, R. R. *J. Am. Chem. Soc.* **1988**, *110*, 4964.
(27) Wallace, K. C.; Davis, W. M.; Schrock, R. R. *Inorg. Chem.* **1990**, *29*, 1104.
(28) Huheey, J. E.; Keiter, E. A.; Keiter, R. L. *Inorganic Chemistry*; Harper Collins College Publishers: New York, 1993.
(29) Chisholm, M. H.; Rothwell, I. P. in *Comprehensive Coordination Chemistry*; Wilkinson, G., Gillard, R. D., McCleverty, J., Eds.; Pergamon Press: Oxford, 1987; Vol. 2, pp 161−188.
(30) Coffindaffer, T. W.; Steffey, B. D.; Rothwell, I. P.; Folting, K.; Huffman, J. C.; Streib, W. E. *J. Am. Chem. Soc.* **1989**, *111*, 4742.
(31) Kerschner, J. L.; Fanwick, P. E.; Rothwell, I. P.; Huffman, J. C. *Inorg. Chem.* **1989**, *28*, 780.
(32) Chisholm, M. H. *Chemtracts: Inorg. Chem.* **1992**, *4*, 273.
(33) Steffey, B. D.; Fanwick, P. E.; Rothwell, I. P. *Polyhedron* **1990**, *9*, 963.
(34) We believe these values of r_O and r_S obtained from internal measurements are more reliable in this simple analysis than values of $r_O = 0.73$ Å and $r_S = 1.02$ Å obtained from other sources (see ref 28 and references therein). Using these values of r_O and r_S further augments the difference between Ta−O vs Ta−S shortening from bond lengths expected on the basis of single bonding only. Thus, the Ta−O bond is ca. 15% shorter than predicted, while the Ta−S bond is ca. 4% shorter than expected.
(35) Smith, G. D.; Fanwick, P. E.; Rothwell, I. P. *Inorg. Chem.* **1990**, *29*, 3221.
(36) Healy, M. D.; Power, M. B.; Barron, A. R. *Coord. Chem. Rev.* **1994**, *130*, 63.

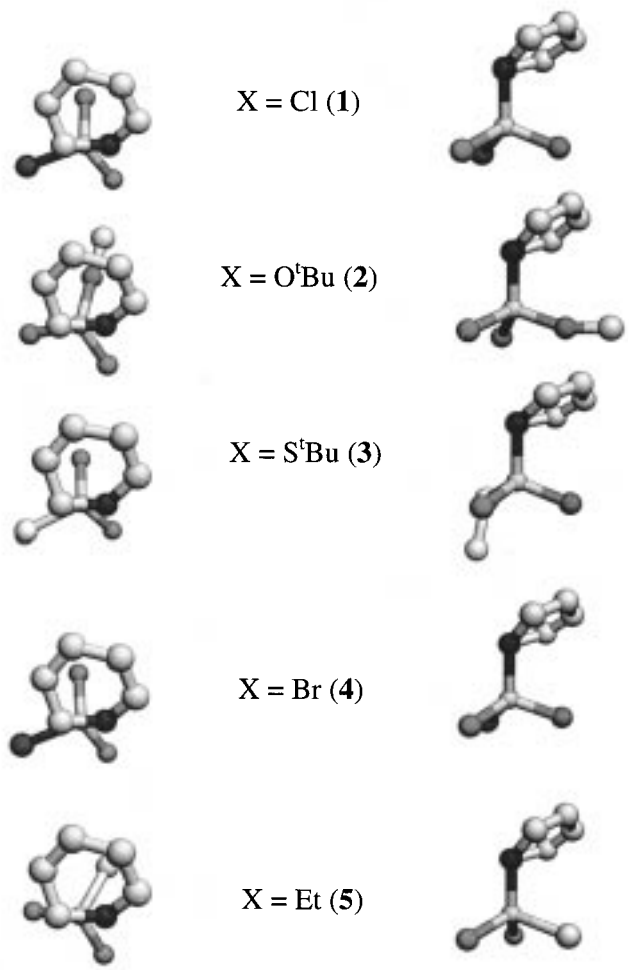

Figure 5. Comparison of the core molecular structures of $[\eta^2(N,C)\text{-}NC_5{}^tBu_3H_2]Ta(OAr)_2X$, where X = Cl (**1**), O^{t}Bu (**2**), S^{t}Bu (**3**), Br (**4**), and Et (**5**). The top view is presented along the C−N centroid → Ta vector, and the side view is viewed along the C(1)−N bond in all compounds.

$Ta(OAr)_2Et$ is proximate to N. Figure 5 compares the core structures of compounds **1**−**5** by presenting the $[NC_5]TaO_2X$ atoms only from two perspectives. The "top" view is presented along the C−N centroid−Ta vector, and the "side" view is viewed along the C(1)−N bond in all compounds.

As seen in the top views of Figure 5, the rotational preference of the pyridine ligand with respect to the TaO_2X triangle roughly aligns the pyridine C−N bond with one apex of the triangle while another apex is situated more or less under the pyridine ring. In the chloride (**1**), S^{t}Bu (**3**), and bromide (**4**) complexes, the pyridine C−N bond aligns roughly with these substituents, while in the O^{t}Bu (**2**) and Et (**5**) complexes, the C−N bond aligns more closely with an aryloxide ligand, placing these substituents under the pyridine ring. As emphasized in the side views, one might expect steric interactions to orient the bulkiest ligand away from the pyridine ligand and thereby place smaller ligands beneath the pyridine ring, however in the halide complexes **1** and **4**, the bulkier aryloxide ligand is situated below the η^2-pyridine ring, suggesting an electronic rather than steric basis for the preferred geometry.

If we consider the C═N bond[37] as occupying a single coordination site, then we can examine these complexes according to Gibson's formalism for tetrahedral complexes with a single Π_1-type ligand—viz., the C═N bond itself that interacts with the metal with a single π bond—and use its orientation to evaluate the π-donor capabilities of the attendant ligands.[38,39] In cases with *two* dominant Π_2 ligands, i.e., ligands that can interact with two π-symmetry orbitals,[38] the Π_1 C═N bond is expected to align toward the weakest π donor in the TaO_2X triangle, as indicated in structure **A** in Figure 6. In cases with one dominant Π_2 ligand, the Π_1 C═N bond should align perpendicular to the M−L bond of this governing Π_2 ligand, as shown in structure **B** of Figure 6. Thus, Gibson's considerations predict the C═N bond will orient either directly aligned *with* the weakest π donor or *side-on* to a single, dominant, strong π donor. We note that OAr, O^{t}Bu, S^{t}Bu, Cl, and Br ligands all may be considered potential Π_2 ligands.

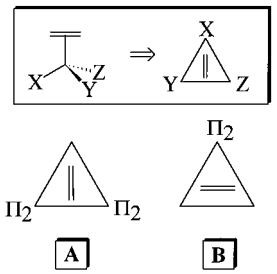

Figure 6. Idealized rotational orientations of a Π_1, doubly bonded ligand such as C═N with respect to the TaO_2X triangle. Shown are the predicted orientations in the presence of *two* dominant Π_2 ligands (A) and in the presence of *one* dominant Π_2 ligand (B).

To more closely identify the structure adopted by each compound, we report the C(1)−N−Ta−L torsion angles in Table 3, where ligand "L" is the atom of the tripodal ligand most closely aligned with the C−N bond of each structure. For structure **A**, we would expect a near 0° C(1)−N−Ta−L torsion angle, whereas structure **B** would provide a torsion angle near 30°, since in either case this angle is measured irrespective of whether the ligand most closely aligned with the C−N bond is a Π_2 ligand. The torsion angle data in Table 3 suggest that complexes **1**, **3**, and **4** are more consistent with structure **A** while complex **5** is closer to structure **B**. The C(1)−N−Ta−L torsion angle in the O^{t}Bu complex **2** (15.5(2)°) does not allow a ready assignment since it suggests a structure halfway between **A** and **B**. Caution must be exercised in making and interpreting these structural assignments, since discerning between idealized structures **A** and **B** is not always straightforward when the tripodal L−M−L angles are inequivalent, as they are in all of these compounds.

For stucture **A**, the Π_1 C═N bond is expected to align toward the weakest π donor in the TaO_2X triangle. Thus, in the complexes $[\eta^2(N,C)\text{-}NC_5{}^tBu_3H_2]Ta(OAr)_2X$ for X = Cl (**1**), S^{t}Bu (**3**), and Br (**4**), the alignment of the Π_1 C═N bond with the Ta−X bond suggests that Cl, S^{t}Bu, and Br are all weaker π donors than an aryloxide ligand. Although *tert*-butylthiolate is a good

(37) We will formally consider this a C═N double bond, on the basis of the extensive π back-bonding into this moiety, as evidenced by the extreme π localization within the pyridine ring. As described in detail above, this bond is significantly reduced to approach a single bond in length.

(38) Gibson, V. C. *Angew. Chem., Int. Ed. Engl.* **1994**, *33*, 1565.
(39) Gibson, V. C. *J. Chem. Soc., Dalton Trans.* **1994**, 1607.

donor ligand as described above, one could argue that OAr ligands in $[\eta^2(N,C)\text{-}NC_5{}^tBu_3H_2]Ta(OAr)_2(S^tBu)$ (**3**) are functioning as better π donors. The structure of the *tert*-butoxide complex $[\eta^2(N,C)\text{-}NC_5{}^tBu_3H_2]Ta(OAr)_2(O^tBu)$ (**2**) reveals the C=N bond aligned *perpendicular* to the Ta−O^{t}Bu linkage, similar to **B** of Figure 6 and consistent with the notion that a *tert*-butoxide ligand functions as a better π donor than an aryloxide.[24,29,40] Therefore, according to Gibson's model, the π-donor (only) capabilities among these ligands decreases as O^{t}Bu > OAr > S^{t}Bu. We emphasize this model pertains to π-donor abilities only, since the Ta−C(1) bond lengths in S^{t}Bu complex **3** (2.24(1) Å) vs the O^{t}Bu species **2** (2.163(3) Å) suggest the S^{t}Bu derivative may be a better $\sigma + \pi$ donor overall. The only compound that does not readily conform to this model is the ethyl complex $[\eta^2(N,C)\text{-}NC_5{}^tBu_3H_2]Ta(OAr)_2Et$ (**5**), for reasons that are not immediately apparent.

Finally, Table 3 also includes the C(5)−N−C(1)−C(2) torsion angle in the η^2-pyridine ligand for complexes **1**−**5**, which may afford some indication of the extent of pyridine distortion and interruption of its aromaticity. If one assumes that the C(5)−N−C(1)−C(2) torsion angle indicates the magnitude of interruption of aromaticity in pyridine, then there appears to be some correlation between this torsion angle and the Ta−C(1) bond distance. Thus, as the Ta−C(1) bond distance decreases, the extent of disruption of the aromaticity in the pyridine ring increases. The Ta−C(1) bond distance presumably corresponds to how tightly the η^2-pyridine is bound to the metal, which is consistent with the concept of more electron density transferred from the formal d^2 metal to the pyridine ligand and a greater interference in the pyridine's aromaticity. In this case, the S^{t}Bu compound **3** appears to have a relatively less distorted and more loosely bound η^2-pyridine ligand as compared to all the other compounds.

Discussion

Wolczanski and co-workers have reported an extended Hückel molecular orbital study[22] of $[\eta^2(N,C)\text{-}NC_5H_5]Ta(OH)_3$ as a model complex for $[\eta^2(N,C)\text{-}NC_5H_5]Ta(OSi^tBu_3)_3$,[21,22] which revealed the origins of η^2 stability over η^6 or η^1 coordination. First, the η^2 mode is favored since it can engage in π-back-bonding interactions with the highly reducing d^2 $Ta(OH)_3$ moiety rather than the less-efficient δ back-bonding in the η^6 mode,[41] thereby allowing the metal to achieve its highest oxidation state. Second, η^2 bonding avoids the destabilizing interaction between the filled $Ta(OH)_3$ d_{z^2} orbital and the pyridine N-donor orbital which would arise from the σ-only interactions of an η^1 mode. Finally, it was discovered that distorting the pyridine α hydrogen out of the pyridine plane, i.e., pyramidalization about the α carbon, is important in stabilizing the η^2 structure in $[\eta^2(N,C)\text{-}NC_5H_5]Ta(OH)_3$.[22] The C_α (i.e., C(1)) position in our complexes $[\eta^2(N,C)\text{-}NC_5{}^tBu_3H_2]Ta(OAr)_2X$ is *tert*-butyl-substituted, and pyramidalization about this C_α is obvious as the *tert*-butyl substituent is considerably displaced from the best pyridine plane. While this distortion must be sterically enhanced, it is consistent with the most electronically favored structure uncovered by Wolczanski and co-workers.

The correlation between the C(5)−N−C(1)−C(2) torsion angle—which we propose indicates the degree of interruption of aromaticity—and the Ta−C(1) bond distance—which we propose measures how tightly the model substrate is bound to the metal—provides an interesting suggestion regarding HDN catalysis. The longest Ta−C(1) distance and the smallest C(5)−N−C(1)−C(2) torsion angle are found in the sulfur-supported derivative $[\eta^2(N,C)\text{-}NC_5{}^tBu_3H_2]Ta(OAr)_2(S^tBu)$ (**3**), therefore this sulfur-supported complex appears to bind the pyridine less tightly than its oxygen homologue. This observation may be relevant to some obervations of Satterfield and co-workers regarding quinoline HDN over sulfided Ni/Mo supported on γ-Al_2O_3.[42−44] The most active site of this catalyst appears to be crystallites of MoS_2, the edges of which are decorated with nickel atoms.[4] Satterfield and co-workers report that the rate of *hydrogenation* reactions is reduced in the presence of added H_2S, but *hydrogenolysis* reactions—and therefore overall denitrogenation—are accelerated under these conditions. It is possible that H_2S plays a role in regenerating the active site rapidly and achieving maximum sulfur coordination of the substrate−catalyst complex. Maximum sulfur coordination would be expected to "deactivate" the catalyst sufficiently to discourage unsaturated hydrocarbons from binding strongly and being reduced while sustaining the catalysts' ability to bind nitrogen compounds just strongly enough for C−N bond cleavage to ensue. Under these conditions, aromatic hydrocarbons compete less effectively for active sites, thereby enhancing the overall rate of nitrogen removal.

Conclusions

This structural study allows us to draw the following conclusions and suggest the extent to which this system is a valid reactivity model for the active site in HDN catalysts.

(1) We have previously established that the $\eta^2(N,C)$ coordination mode exists only in the d^2 oxidation state and demonstrated that C−N bond cleavage occurs only in the $\eta^2(N,C)$-pyridine complexes, therefore systems containing $\eta^2(N,C)$-bound heterocycles appear to be relevant as a *reactivity* model for HDN catalysis.

(2) Structural evidence clearly demonstrates a disruption of aromaticity of these substituted $\eta^2(N,C)$-pyridine compounds. Because the $\eta^2(C,C)$-pyridine or $\eta^2(C,C)$-quinoline coordination modes have not been observed in d^2 tantalum complexes, this interruption of aromaticity accompanies a selective activation of the heterocycle's C−N bond, therefore these species constitute good *structural* models for the substrate−catalyst adduct in HDN catalysis.

(3) A structural comparison of $\eta^2(N,C)$-pyridine ligands in oxygen- vs sulfur-supported complexes suggests that

(40) Chisholm, M. H.; Clark, D. L. *Comm. Inorg. Chem.* **1987**, *6*, 23.
(41) Arney, D. J.; Wexler, P. A.; Wigley, D. E. *Organometallics* **1990**, *9*, 1282.
(42) Satterfield, C. N.; Gültekin, S. *Ind. Eng. Chem. Process Des. Dev.* **1981**, *20*, 62.
(43) Yang, S. H.; Satterfield, C. N. *Ind. Eng. Chem. Process Des. Dev.* **1984**, *23*, 20.
(44) Satterfield, C. N.; Smith, C. M.; Ingalls, M. *Ind. Eng. Chem. Process Des. Dev.* **1985**, *24*, 1000.

although sulfur ligands may be better $\sigma + \pi$ donor ligands overall, the analogous oxygen ligand appears to be a better π-donor ligand. Thus, the π-donor (only) capabilities among these ligands decreases as O^{t}Bu > OAr > S^{t}Bu.

(4) The $\eta^2(N,C)$-pyridine ligand in the sulfur-supported complex appears to be more loosely bound than in its oxygen-supported homologue. Therefore, sulfur coordination may impart the precise catalyst activity required to prevent unsaturated hydrocarbons from binding very tightly while sustaining the catalysts' ability to bind nitrogen compounds strongly enough for reduction and C−N bond cleavage to ensue.

Experimental Section

General Details. All experiments were performed under a nitrogen atmosphere either by standard Schlenk techniques[45] or in a Vacuum Atmospheres HE-493 drybox at room temperature (unless otherwise indicated). Solvents were distilled under N_2 from an appropriate drying agent[46] and were transferred to the drybox without exposure to air. NMR solvents were passed down a short (5−6 cm) column of activated alumina prior to use. Abbreviations: Ar = 2,6-$C_6H_3{}^iPr_2$.

Physical Measurements. ^{1}H and ^{13}C NMR spectra were recorded at probe temperature (unless otherwise specified) on a Bruker AM-250 or Varian Unity 300 spectrometer in C_6D_6 solvent. Chemical shifts are referenced to protio impurities (δ 7.15) or solvent ^{13}C resonances (δ 128.0) and are reported downfield of $SiMe_4$. Routine coupling constants are not reported. NMR assignments were assisted by HETCOR, HMQC, HMBC, and NOESY spectra. Electron ionization mass spectra (70 eV) were recorded to $m/z = 999$ on a Hewlett-Packard 5970 mass selective detector and RTE-6/VM data system. Microanalytical samples were handled under nitrogen and were combusted with WO_3 (Desert Analytics, Tucson, AZ).

Starting Materials. $[\eta^2(N,C)$-$NC_5{}^tBu_3H_2]Ta(OAr)_2Cl$ (**1**) was prepared as previously described.[18] The reagents HO^{t}Bu, HS^{t}Bu, ^{n}BuLi, and KH were obtained from Aldrich and used as received. KO^{t}Bu was prepared from HO^{t}Bu and KH, and LiS^{t}Bu was prepared from ^{n}BuLi and HS^{t}Bu in hydrocarbon solvents.

Preparations. $[\eta^2(N,C)$-$NC_5{}^tBu_3H_2]Ta(OAr)_2(O^tBu)$ (2). A THF solution of KO^{t}Bu (0.069 g, 0.61 mmol, 20 mL of THF) was slowly added to a stirred solution of $[\eta^2(N,C)$-$NC_5{}^tBu_3H_2]Ta(OAr)_2Cl$ (0.50 g, 0.61 mmol) in 5 mL of THF. The red solution developed an orange color over the course of the addition. After 18 h, the mixture was filtered through Celite and the reaction volatiles were removed from the filtrate under reduced pressure to afford an orange oil. Trituration of this oil with a minimal volume of Et_2O induced crystallization. The resulting solid was filtered off and dried in vacuo to afford 0.43 g (0.50 mmol, 81%) of product as orange microcrystals. Analytically pure compound was obtained as orange crystals by layering acetonitrile over a solution of **2** in minimal Et_2O and storing the solution at −35 °C. ^{1}H NMR (C_6D_6): δ 7.11, 7.10 (overlapping pseudo d, A_2B mult, 4 H total, H_{aryl}), 6.98, 6.96 (overlapping pseudo t, A_2B mult, 2 H total, H_{aryl}), 6.05 (s, 1 H, H5), 5.46 (s, 1 H, H3), 3.83, 3.38 (b, 2 H each, C*H*Me$_2$), 1.42 (s, 9 H, C6CMe$_3$), 1.28 (s, 9 H, C4CMe$_3$), 1.27, 1.24, 1.19, 1.10 (d, 6 H each, CH*Me*$_2$), 1.23 (s, 9 H, OCMe$_3$), 0.86 (s, 9 H, C2CMe$_3$). ^{13}C NMR (C_6D_6): δ 167.79 (C6), 158.55, 157.34 (C_{ipso} OAr), 142.43 (C4), 138.29, 138.02 (C_o OAr), 123.89, 123.44 (C_m OAr), 122.80 (C_p OAr), 113.02 (C5), 106.35 (C2), 99.82 (C3), 86.91 (O*C*Me$_3$), 41.48 (C6*C*Me$_3$), 37.49 (C2*C*Me$_3$), 34.45 (C4*C*Me$_3$), 31.37 (OC*Me*$_3$), 30.37 (C4*C*Me$_3$), 29.48 (C2C*Me*$_3$), 28.00 (C6*C*Me$_3$), 26.90, 26.70 (*C*HMe$_2$), 24.60, 23.85 (CH*Me*$_2$). One C_p OAr resonance is not observed and is either coincident with the δ 122.80 (C_p OAr) signal or obscured by solvent resonances. Anal. Calcd for $C_{45}H_{72}NO_3Ta$: C, 63.14; H, 8.48; N, 1.64. Found: C, 63.14; H, 8.29; N, 1.38.

$[\eta^2(N,C)$-$NC_5{}^tBu_3H_2]Ta(OAr)_2(S^tBu)$ (3). A solution of LiS^{t}Bu (0.116 g, 1.21 mmol) in 15 mL of Et_2O was slowly added to a stirred solution of $[\eta^2(N,C)$-$NC_5{}^tBu_3H_2]Ta(OAr)_2Cl$ (1.00 g, 1.22 mmol) in 5 mL of Et_2O. The red solution became orange in color over the course of the addition. After 24 h, the reaction mixture was filtered through Celite and the reaction volatiles were removed from the filtrate under reduced pressure, yielding a red-orange oil. Trituration of this oil with minimal Et_2O induced crystallization. The resulting solid was collected by filtration and dried in vacuo to afford 0.61 g (0.70 mmol, 58%) of product as red crystals. The volume of the filtrate was reduced, acetonitrile was added, and the solution stored at −35 °C to provide an additional 0.10 g (0.11 mmol) of red crystals, which were suitable for elemental analysis and X-ray crystallography; total yield 0.71 g (0.81 mmol, 67%). ^{1}H NMR (C_6D_6; x = C2 or C6, y = C6 or C2): δ 7.13−6.82 (two overlapping A_2B mult, 6 H total, H_{aryl}), 6.35 (s, 1 H, H5), 5.51 (s, 1 H, H3), 4.08, 3.26 (br, 1 H each, C*H*Me$_2$), 3.71 (spt, 2 H, C*H*Me$_2$), 1.51 (s, 9 H, SCMe$_3$), 1.44 (s, 9 H, C*x*CMe$_3$), 1.32 (s, 9 H, C4CMe$_3$), 1.27 (overlapping br and d, 24 H, CH*Me*$_2$), 0.81 (s, 9 H, C*y*CMe$_3$). ^{13}C NMR (C_6D_6; x = C2 or C6, y = C6 or C2): δ 167.84 (C6), 158.00, 157.02 (C_{ipso} OAr), 143.94 (C4), 138.96 (C_o OAr), 124.33, 124.01 (C_m OAr), 123.64 (C_p OAr), 115.25 (C5), 104.77 (C2), 101.49 (C3), 48.22 (S*C*Me$_3$), 43.00 (C*xC*Me$_3$), 38.60 (C*yC*Me$_3$), 35.60 (SC*Me*$_3$), 34.32(C4*C*Me$_3$), 30.70 (C4C*Me*$_3$), 29.25 (CyC*Me*$_3$), 28.99 (C*x*C*Me*$_3$), 26.80, 24.67 (*C*HMe$_2$), 26.02, 24.10 (CH*Me*$_2$). One C_o OAr and one C_p OAr resonance are not observed and are either coincident with another signal or obscured by solvent resonances. Anal. Calcd for $C_{45}H_{72}NO_2STa$: C, 61.96; H, 8.33; N, 1.61. Found: C, 62.15; H, 8.27; N, 1.67.

$[\eta^2(N,C)$-$NC_5{}^tBu_3H_2]Ta(OAr)_2Br$ (4). A solution of $[\eta^2(N,C)$-$NC_5{}^tBu_3H_2]Ta(OAr)_2Cl$ (1.00 g, 1.22 mmol) in 25 mL of THF was prepared and rapidly stirred while an EtMgBr solution was added (0.611 mL of a 2 M Et_2O solution, 1.22 mmol). This reaction mixture was stirred for 24 h, over which time it developed a light orange color. The reaction volatiles were then removed under reduced pressure to afford a red-orange oil. This oil was dissolved in cold pentane (ca. −30 °C) and filtered through Celite to remove the white precipitate that formed upon pentane addition. The orange filtrate was stripped of solvent in vacuo to provide an orange oil, which is shown by ^{1}H NMR to be a relatively pure sample of the ethyl derivative $[\eta^2(N,C)$-$NC_5{}^tBu_3H_2]Ta(OAr)_2Et$ (**5**).[13] This oil was dissolved in a minimal volume of pentane (ca. 1 mL) and cooled to −35 °C. After 3 days, a few red crystals (shown by X-ray diffraction to be $[\eta^2(N,C)$-$NC_5{}^tBu_3H_2]Ta(OAr)_2Br$) had formed from the orange solution. These crystals were collected by filtration and dried in vacuo to provide only a trace yield. The low isolated yield of this compound has precluded its spectroscopic and analytical characterization. The major product of this reaction, $[\eta^2(N,C)$-$NC_5{}^tBu_3H_2]Ta(OAr)_2Et$ (**5**), can be crystallized from Et_2O/MeCN solutions as previously described.[13]

X-ray Crystallographic Studies. General. Scattering factors were taken from Cromer and Waber.[47] Anomalous dispersion effects were included in F_c;[48] the values for $\Delta f'$ and $\Delta f''$ were those of Cromer.[49] The scan range (ω) was deter-

(45) Shriver, D. F.; Drezdzon, M. A. *The Manipulation of Air-Sensitive Compounds*, 2nd ed.; John Wiley and Sons: New York, 1986.
(46) Perrin, D. D.; Armarego, W. L. F. *Purification of Laboratory Chemicals*, 3rd ed.; Pergamon Press: Oxford, 1988.
(47) Cromer, D. T.; Waber, J. T. *International Tables for X-ray Crystallography*; The Kynoch Press: Birmingham, England, 1974; Vol. IV, Table 2.2B.
(48) Ibers, J. A.; Hamilton, W. C. *Acta Crystallogr.* **1964**, *7*, 781.
(49) Cromer, D. T. *International Tables for X-ray Crystallography*; The Kynoch Press: Birmingham, England, 1974; Vol. IV, Table 2.3.1.

mined as a function of θ to correct for the separation of the Kα doublet (CAD4 Operations Manual, 1977). All calculations were performed on a VAX computer using MolEN. Details of the structural determination and refinement are reported in Table 1.

[η^2(*N,C*)-NC$_5$^{t}Bu$_3$H$_2$]Ta(OAr)$_2$(O^{t}Bu) (2). An orange, block-shaped crystal of **2**, crystallized from Et_2O/MeCN (−35 °C) having approximate dimensions of 0.33 × 0.33 × 0.50 mm, was immersed in Paratone-N and mounted on a glass fiber in a random orientation under a cold stream of N_2. Cell constants and an orientation matrix for data collection were obtained from least-squares refinement, using the setting angles of 25 reflections in the range $30° < 2\theta < 40°$. From the systematic absences of $h0l$ h + l = $2n + 1$ and $0k0$ $k = 2n + 1$ and from subsequent least-squares refinement, the space group was determined to be $P2_1/n$ (No. 14). Hydrogen positions were determined from difference maps and then idealized. Hydrogen atoms were included in the refinement but constrained to ride on the atom to which they are bonded.

[η^2(*N,C*)-NC$_5$^{t}Bu$_3$H$_2$]Ta(OAr)$_2$(S^{t}Bu) (3). A red, monoclinic, block crystal of **3** was crystallized from Et_2O/MeCN solution (−35 °C) and was mounted in a glass capillary with its long axis roughly parallel to the φ axis of the goniometer. Cell constants and an orientation matrix for data collection were obtained from least-squares refinement, using the setting angles of 25 reflections in the range $18 < 2\theta < 40°$. From the systematic absences of $h00$ $h = 2n + 1$, $0k0$ $k = 2n + 1$ and $00l$ $l = 2n + 1$ and from subsequent least-squares refinement, the space group was determined to be $P2_12_12_1$ (No. 19). Many hydrogen atoms were visible in succeeding difference Fourier syntheses; all non-methyl hydrogen atoms were added at idealized positions. Methyl hydrogens, except those on C(1C), were added starting with the positions found in the difference maps to determine the orientation and then idealized. No hydrogen positions were visible for C(1C), so hydrogens were added to this methyl group in a staggered configuration. All hydrogen atoms were included in the refinement but constrained to ride on the atom to which they are bonded.

[η^2(*N,C*)-NC$_5$^{t}Bu$_3$H$_2$]Ta(OAr)$_2$Br (4). A dark red, rectangular block crystal of **4** was crystallized from pentane solution (−35 °C) and was mounted in a glass capillary in a random orientation. Cell constants and an orientation matrix for data collection were obtained from least-squares refinement, using the setting angles of 25 reflections in the range $10° < 2\theta < 18°$. From the systematic absences of $h0l$ $h = 2n + 1$ and $0kl$ $l = 2n + 1$ and from subsequent least-squares refinement, the space group was determined to be $Pca2_1$ (No. 29). Hydrogen atoms were included in the refinement but constrained to ride on the atom to which they are bonded.

Acknowledgment is made to the Division of Chemical Sciences, Office of Basic Energy Sciences, Office of Energy Research, U.S. Department of Energy (Grant No. DE-FG03-93ER14349), for support of this research.

Supporting Information Available: Complete crystallographic details, including tables of atomic positional and thermal parameters, bond distances and angles, least-squares planes, and dihedral angles and ORTEP figures for [η^2(*N,C*)-NC$_5$^{t}Bu$_3$H$_2$]Ta(OAr)$_2$(O^{t}Bu) (**2**), [η^2(*N,C*)-NC$_5$^{t}Bu$_3$H$_2$]Ta(OAr)$_2$(S^{t}Bu) (**3**), and [η^2(*N,C*)-NC$_5$^{t}Bu$_3$H$_2$]Ta(OAr)$_2$Br (**4**) (67 pages). Ordering information is given on any current masthead page.

OM970559G